

Energy Conversion in Magnetic Reconnection with Chaos Diffusion

Hiroaki OHTANI^{1,2)}, Wendell HORTON³⁾, Tomio PETROSKY⁴⁾ and Ritoku HORIUCHI^{1,2)}

¹⁾*National Institute for Fusion Science, Toki 509-5292, Japan*

²⁾*The Graduate University for Advanced Studies (SOKENDAI), Toki 509-5292, Japan*

³⁾*Institute of Fusion Studies, University of Texas at Austin, TX 78712, USA*

⁴⁾*Center for Complex Quantum Systems, University of Texas at Austin, TX 78712, USA*

(Received: 28 August 2008 / Accepted: 21 November 2008)

Electromagnetic particle simulation is performed in order to investigate the behavior of collisionless driven reconnection in an open system. Ion frozen-in condition in the vicinity of magnetic neutral sheet is broken due to the growth of off-diagonal components of pressure tensor term. The relationship between the pressure tensor and the meandering motion in the ion dissipation region is clarified based on a simple model. The energy conversions to electron and ion energies occur actively in the vicinity of the reconnection region and in the downstream region, respectively. The field energy is converted to particle energy due to the reconnection process and the ratio of the ion thermal energy to the total energy in the outflow is in good agreement with the observation by the Geotail satellite.

Keywords: Magnetic reconnection, Particle simulation, Pressure tensor, Energy conversion

1 Introduction

Collisionless magnetic reconnection is widely considered to play an important role in energetically active phenomena in high temperature plasmas. In spite of intensive research, many basic questions about the details of mechanism of collisionless reconnection still remain poorly understood. To investigate the behavior of collisionless reconnection, we have developed a PIC code (PASMO) in an open system [1–3]. Ions become unmagnetized and execute a complex thermal motion called meandering in the ion dissipation region. The complex meandering (chaotic) motion leads to the growth of off-diagonal components of the pressure tensor term, which is one of main causes to break ion frozen-in condition in the vicinity of magnetic neutral sheet [4, 5]. In this study, we investigate the role of the meandering motion in the formation of ion dissipation region by examining particle simulation results of collisionless driven reconnection based on a simple model. Moreover we report the energy conversion to electrons and ions passing through the dissipation region.

2 Simulation model

The three-dimensional simulation code PASMO [1–3] relies on an explicit electromagnetic PIC method. Simulation parameters are as follows; The simulation box size is $2032\lambda_D \times 127\lambda_D \times 48\lambda_D$, where λ_D is Debye length. The total number of particles is 153.6 million,

the scale length of current layer L is $25\lambda_D$, the ratio of the particle density of background plasmas to that of foreground plasmas is 0.2 at the initial time. The thermal velocities of electron and ion are $0.26c$ and $0.026c$, respectively, where c is the speed of light. The mass ratio m_i/m_e is 100. The initial condition is given by a one-dimensional Harris-type equilibrium, in which the magnetic field is parallel to x -axis and a function of y -coordinate. At the upstream boundary (y boundary), ions and electrons enter into the system with $\mathbf{E} \times \mathbf{B}$ drift due to a driving electric field E_{z0} , whereas at the downstream boundary (x boundary), particles exit from and enter into the system under the free boundary condition. The external driving electric field $E_{zd}(x, t)$ at the upstream boundary is programmed to evolve from zero to a constant value during an early period. The field E_{zd} is set for zero at $t = 0$ and gradually increases predominantly in the center region of the simulation box ($x = 0$) in the early time. The width of the region where E_{zd} predominantly increases is also gradually expanded. The field E_{zd} develops on the whole boundary after it attains to a constant value E_0 at the center point, and then it reaches to E_0 on the whole boundary. After an early phase ($t\omega_{ce} = 335$ in our simulation, where ω_{ce} is a electron cyclotron frequency), E_{zd} keeps a constant value E_0 which is a necessary condition for a reconnection system to evolve toward a steady state, in which all the profiles are almost kept unchanged with time [1].

author's e-mail: ohtani@dss.nifs.ac.jp

3 Temporal evolution

Figure 1 shows isosurface of $B_x^2 + B_y^2$ and magnetic field streamline at (a) $t\omega_{ce} = 0$, (b) 550.01, (c) 608.59, and (d) 805.53, respectively. The plasma inflow and magnetic flux go from the upstream toward the center region because of the driving electric field E_{z0} imposed at the upstream boundary. The driving field penetrates into the current sheet owing to particle kinetic effects, and triggers magnetic reconnection when it reaches the center (Fig. 1(b)) [6–8]. Since the length of current sheet is much longer than its width, the tearing instability is excited in the downstream region, several reconnection points appear and then several magnetic islands are generated (Fig. 1(c)). The magnetic islands become unstable against a kink instability [9].

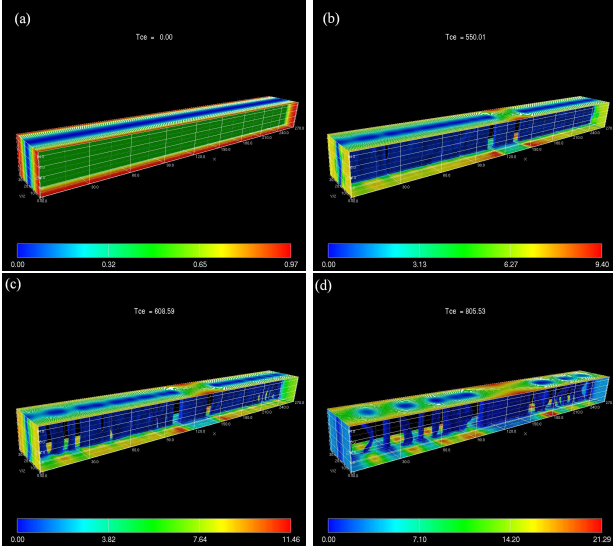


Fig. 1 Isosurface of $B_x^2 + B_y^2$ and magnetic field streamline at (a) $t\omega_{ce} = 0$, (b) 550.01, (c) 608.59, and (d) 805.53.

4 Pressure tensor term

We focus on the ion dissipation region around the central reconnection point at which collisionless reconnection sets in first under the influence of driving flow. Let us consider the mechanism which breaks down the ion frozen-in condition in the collisionless reconnection by examining the force balance equation for ions as

$$\begin{aligned} & E_z + (u \times B)_z \\ &= \frac{m}{q} \left\{ \frac{\partial}{\partial t} + (u \cdot \nabla) \right\} u_z \\ &+ \frac{1}{qn} \left(\frac{\partial \Pi_{xz}}{\partial x} + \frac{\partial \Pi_{yz}}{\partial y} \right), \end{aligned} \quad (1)$$

where m is mass, q is charge, n is number density, Π_{ij} is pressure tensor, and u_i is flow velocity. Figure 2

demonstrates the spatial profiles of the each terms of Eq. (1) along the inflow (y) direction through the reconnection point ($x = 0$). It is clearly seen in Fig. 2 that the pressure tensor term $\frac{1}{qn} \frac{\partial \Pi_{yz}}{\partial y}$ mainly sustains the electric field E_z around the reconnection point.

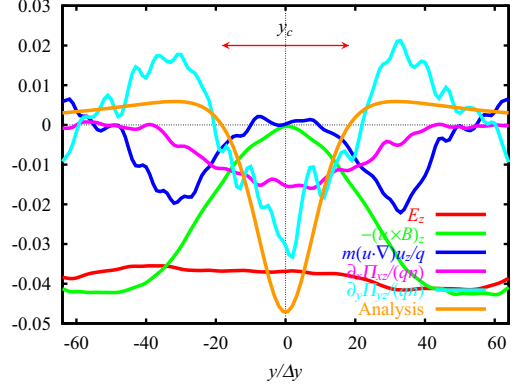


Fig. 2 Spatial profiles of terms of the force balance equation for ion and analytic solution of $\frac{1}{qn} \frac{\partial \Pi_{yz}}{\partial y}$ along y direction through the reconnection point. Red, green, blue, magenta, sky blue and orange lines show E_z , $-(u \times B)_z$, $m(u \cdot \nabla)u_z/q$, $\frac{1}{qn} \frac{\partial \Pi_{xz}}{\partial x}$, $\frac{1}{qn} \frac{\partial \Pi_{yz}}{\partial y}$ in the simulation result, and analytic solution of $\frac{1}{qn} \frac{\partial \Pi_{yz}}{\partial y}$, respectively.

Pressure tensor originates from the stochastic thermal motion called meandering in the vicinity of reconnection point. Here we examine the relationship between the meandering motion and the pressure tensor based on a simple model. Roughly speaking meandering motion near the reconnection point consists of the motion along the inflow direction (y direction), and along the outflow direction (x direction). The average orbit amplitudes of the meandering motion L_m^y along the inflow direction and L_m^x along the outflow direction are determined from the location which satisfies the relation [1]

$$L_m^y = \rho_L^y(L_m^y), L_m^x = \rho_L^x(L_m^x), \quad (2)$$

where the local ion Larmor radii $\rho_L^y(y)$ along the inflow direction and $\rho_L^x(x)$ along the outflow direction are defined as

$$\begin{aligned} \rho_L^y(y) &= \frac{mv_{\perp}}{qB_x} \simeq \frac{mv_{th}}{qB'_x y}, \\ \rho_L^x(x) &= \frac{mv_{\perp}}{qB_y} \simeq \frac{mv_{th}}{qB'_y x}, \end{aligned} \quad (3)$$

with the thermal velocity v_{th} and constant parameters B'_x and B'_y . In deriving Eq. (3), we used the approximated relations as

$$B_x = B'_x y, B_y = B'_y x. \quad (4)$$

Substitute Eq. (3) into Eq. (2), we get the average orbit amplitudes of meandering motion along the y

and x directions as

$$(L_m^y)^2 = \frac{mv_{th}}{qB'_x}, (L_m^x)^2 = \frac{mv_{th}}{qB'_y}. \quad (5)$$

Because the meandering motion is relevant to the dissipation mechanism [5], these two scales are regarded as the width y_c and the length x_c of ion dissipation region.

In order to connect the meandering motion to the pressure tensor, let us write down $\frac{1}{qn} \frac{\partial \Pi_{yz}}{\partial y}$ as a function of y . If the plasma has a significant $E \times B$ flow velocity and is not so hot about its mean value, then the pressure tensor Π_{yz} is approximately given by

$$\Pi_{yz} \sim \int dv m v_y v_z f, \quad (6)$$

where f is the velocity distribution function. This is a type of semi-cold plasma approximation particularly for the y -direction. Since the frozen-in condition is satisfied outside of the dissipation region ($|y| \geq y_c$), the average velocities v_y in the inflow direction and v_z in the current direction are approximately given by $E \times B$ drift velocity and thermal velocity v_{th} at the inflow edge of the ion dissipation region ($|y| = y_c$), respectively. Accordingly, the pressure tensor Π_{yz} in Eq. (6) is written as

$$\Pi_{yz} \sim \frac{mnE_z B_x v_{th}}{B_x^2 + B_y^2}. \quad (7)$$

In the region where B_x changes linearly in y , we can substitute Eq. (4) into Eq. (7). The pressure tensor term $\frac{1}{qn} \frac{\partial \Pi_{yz}}{\partial y}$ in Eq. (1) is given by

$$\frac{1}{qn} \frac{\partial \Pi_{yz}}{\partial y} = -\frac{1}{qn} \frac{mnE_z B'_x v_{th} (B_x'^2 y^2 - B_y^2)}{(B_x'^2 y^2 + B_y^2)^2}. \quad (8)$$

This analytic solution is drawn in Fig. 2 as an orange line. Equation (8) is sensitive to the value of B_y at the null point $B_y = 0$, since it diverges at $y = 0$ for $B_y = 0$. However, the divergence has been removed by the finite size of the orbits averaged over the null point in our simulations, as well as in the kinetic theory. In this simple model, B_y is a constant value ($B_y = 1$ in this paper) in order to study the tendency of the analytic solution. As one can see in Fig. 2, the tendency of this solution is in agreement with the pressure tensor term $\frac{1}{qn} \frac{\partial \Pi_{yz}}{\partial y}$ (a sky blue line) of the simulation result. When we substitute y_c into y in Eq. (8) and ignore the term B_y because $|B_x| \gg |B_y|$, RHS of Eq. (8) is reduced to $-E_z$. This result supports that the meandering motion plays an important role in collisionless reconnection.

5 Energy conversion

Because the temporal change of the total field energy is written by

$$\frac{d}{dt} \int d^3x \left\{ \frac{B^2}{8\pi} + \frac{E^2}{8\pi} \right\}$$

$$= \int d^3x \left\{ \nabla \cdot \left(\frac{B \times E}{4\pi} \right) - E \cdot J \right\}, \quad (9)$$

the energy conversion between the field and the particles in plasma is carried out through the work by electric field, i.e., the term $E \cdot J$ [10]. In order to investigate this conversion process to electrons and ions respectively, let us decompose the total current to the electron and ion current (J_e and J_i). Figures 3 and 4 show the contour maps of energy conversion rate $E \cdot J_e$ and $E \cdot J_i$, which is averaged along z -direction, at (a) $t\omega_{ce} = 475.4$ when the reconnection starts to take place, (b) 533.7, (c) 611.1, and (d) 792.5 in the xy plane, respectively. For comparison between the energy conversion rate and the magnetic field structure, the magnetic flux ϕ is demonstrated in Fig. 5. The magnetic flux ϕ is calculated from the averaged values B_x and B_y along z -direction. When the reconnection takes place at the center region ($t\omega_{ce} = 475.4$), the energy conversion to electron energy $E \cdot J_e$ becomes active in the vicinity of the central reconnection point, and the energy conversion to ion energy $E \cdot J_i$ becomes to be operative in the outflow regions of the central reconnection region. After the tearing instability is excited and the magnetic islands are generated ($t\omega_{ce} > 611$), $E \cdot J_e$ becomes slightly weaker in the vicinity of the central reconnection point and grows in the outflow regions of other reconnection regions. On the other hand, $E \cdot J_i$ keeps strongly active in the outflow regions of the central reconnection region and the active region moves toward the x boundary. In the outflow regions of other reconnection regions, $E \cdot J_i$ also grows but the magnitude is smaller than that in the outflow regions of the central reconnection region.

In the vicinity of the reconnection point, the electric field is dominated by the reconnection field E_z , and acts on the particles. From Fig. 3, it is found that E_z leads mainly to the increase of the electron energy in the vicinity of the reconnection point. In the downstream region, on the other hand, the electric field is the electrostatic component, which grows dominantly in xy plane [10]. From Fig. 4, it is considered that the electrostatic component of the electric field leads to the increase of ion energy in the downstream region. These energy conversions to electron and ion energies keep active in the ion dissipation and downstream regions at the steady state ($t\omega_{ce} = 792.5$), respectively.

Finally, in order to investigate the energy conversion from field to particles by the reconnection process at the steady state, we calculate the magnetic energy (E_B), ion and electron kinetic energy (K_i and K_e), and ion and electron thermal energy ($\frac{3}{2}n_i T_i$, $\frac{3}{2}n_e T_e$) in the inflow and outflow regions of the ion dissipation region, respectively (Table 1). The inflow regions are defined as the boxes ($-x_c/2 < x < x_c/2$

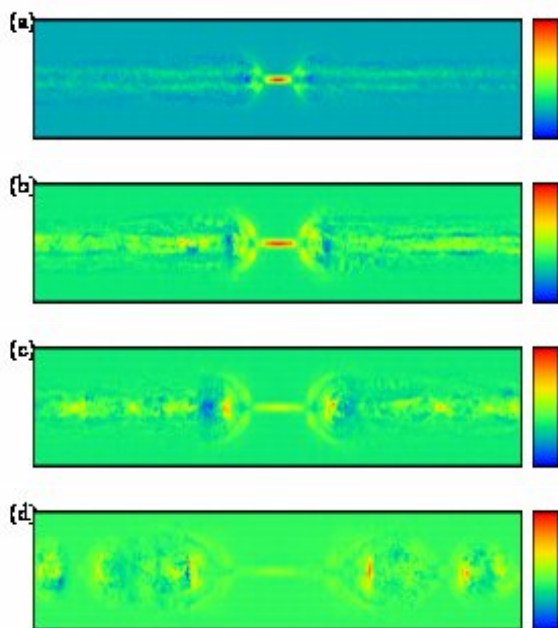


Fig. 3 The contour map of $\mathbf{E} \cdot \mathbf{J}_e$ at (a) $t\omega_{ce} = 475.4$ when the reconnection starts to take place, (b) 533.7, (c) 611.1 and (d) 792.5. Horizontal axis is x , and vertical axis is y . The center region of the simulation box with $1494\lambda_D$ in the x direction is enlarged.

and $-3y_c/2 < y < -y_c/2$, $-x_c/2 < x < x_c/2$ and $y_c/2 < y < 3y_c/2$, and outflow regions as the boxes ($-3x_c/2 < x < -x_c/2$ and $-y_c/2 < y < y_c/2$, $x_c/2 < x < 3x_c/2$ and $-y_c/2 < y < y_c/2$), respectively. Compared with the energies in the inflow region, the magnetic energy in the outflow region is decreased, while the kinetic and thermal energies in the outflow region are increased. It is found that the energy is converted from the magnetic field to particles due to the reconnection process when they pass through the dissipation region. The ratio of the ion thermal energy $\frac{3}{2}n_i T_i$ to the total energy in the outflow is 0.35. This ratio is good agreement with the observation by the Geotail satellite [11].

	E_B	K_i	$\frac{3}{2}n_i T_i$	K_e	$\frac{3}{2}n_e T_e$
inflow	176	51	66	2	60
outflow	51	105	135	38	54

Table 1 Magnetic energy and particle energy in the inflow and outflow regions.

6 Summary

To investigate the behavior of collisionless driven magnetic reconnection, we performed a three-dimensional full electromagnetic particle simulation in an open system using PSMO code. By examining the results, we

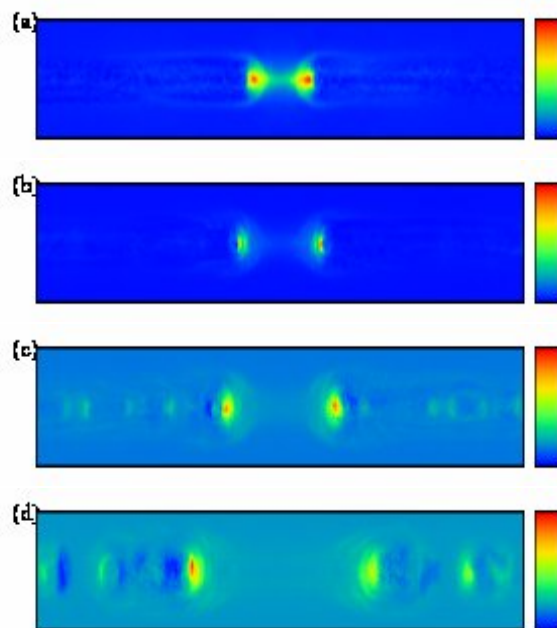


Fig. 4 The same figure as Fig. 3 but for $\mathbf{E} \cdot \mathbf{J}_i$.

recognized that the ion orbit effect (meandering orbit effect) controls the physics in the ion dissipation region from the simple analysis. In the investigation of the energy conversion rate, it is found that the energy conversions to electron and ion energies take place in the vicinity of the reconnection region and the downstream region, respectively.

Acknowledgments

This work is supported by Grant-in-Aids for Scientific Research (No.18340188) and for Young Scientists (B) (No.19740346) from the Japan Society for the Promotion of Science (JSPS), respectively, and the Research Cooperation Program on ‘‘Hierarchy and Holism in Natural Sciences 2’’ at National Institutes of Natural Sciences, and the Department of Energy and the National Science Foundation grant ATM 200502484. And it is also performed with the support and under the auspices of the National Institute for Fusion Science (NIFS) Collaborative Research Program (NIFS08KTAN004).

- [1] W. Pei, R. Horiuchi, T. Sato, *Phys. Plasmas* **8**, 3251 (2001).
- [2] H. Ohtani, S. Ishiguro, R. Horiuchi, Y. Hayashi and N. Horiuchi, *Lecture Notes Comput. Sci.*, **4759**, 329,
- [3] H. Ohtani and R. Horiuchi, submitted to *J. Comput. Phys.*, (2008).
- [4] W. Horton and T. Tajima, *J. Geophys. Res.* **96**, 15811 (1991).
- [5] A. Ishizawa and R. Horiuchi, *Phys. Rev. Lett.* **95**, 045003 (2005).
- [6] R. Horiuchi and H. Ohtani, *Comm. Comp. Phys.* **4**, 496 (2008).

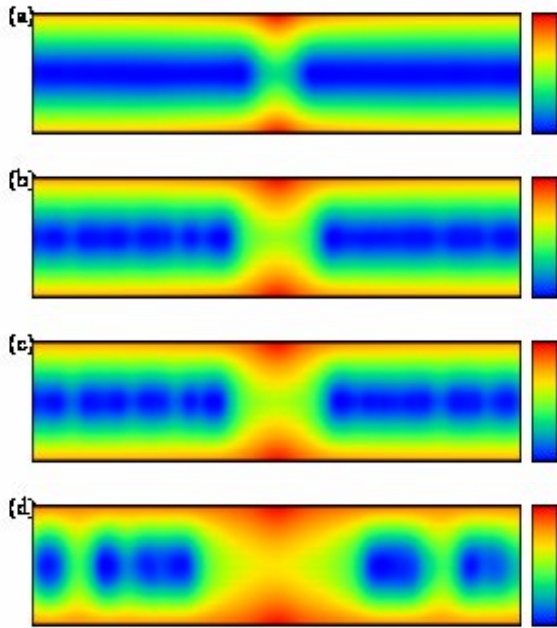


Fig. 5 The same figure as Fig. 3 but for magnetic flux ϕ .

- [7] R. Horiuchi, H. Ohtani, A. Ishizawa, *Comp. Phys. Comm.*, **164**, 17, (2004).
- [8] H. Ohtani, R. Horiuchi and A. Ishizawa, *J. Plasma Phys.* **72**, 929, (2006).
- [9] R. Horiuchi, H. Ohtani and A. Ishizawa, *J. Plasma Phys.* **72**, 953, (2006).
- [10] R. Horiuchi and T. Sato, *Phys. Plasmas* **4**, 277, (1997).
- [11] K. Sigsbee, C. A. Cattell, D. Fairfield, K. Tsuruda, and S. Kokubun, *J. Geophys. Res.* **107(A7)**, 1141, (2002).